Pure & Appl. Chem., Vol. 70, No. 4, pp. 799–808, 1998.
Printed in Great Britain.

Electronic structure contributions to function in bioinorganic chemistry: The blue copper active site

Edward I. Solomon, Louis B. LaCroix, David W. Randall*

Department of Chemistry, Stanford University, Stanford, CA 94305

Abstract: The blue copper site has a unique electronic structure which contributes to its electron transfer function and is reflected in unique spectral properties. The HOMO in the oxidized blue Cu site exhibits high anisotripic covalency which enhances intra- and inter-protein electron transfer rates. The electronic structure of the reduced d^{10} blue Cu centers is developed using a combination of variable energy photoelectron spectroscopy and density functional calculations. These studies establish the change in electronic structure that occurs upon oxidation of the blue Cu center and permit an evaluation of whether the reduced geometry is imposed on the oxidized site by the protein (*i.e.* the entatic/rack state). Studies of the perturbed blue Cu site in nitrite reductase demonstrate that a tetragonal distortion is the origin of the perturbed spectral features of this site. This distortion derives from a Jahn-Teller force along an ~ε(u) mode not present in the classic blue copper proteins and reflects differences in protein contributions to active site structure.

INTRODUCTION

Often considered prototypical electron transfer (ET) proteins, blue copper proteins use the Cu(II)/Cu(I) redox couple to perform this critical biological function on both an inter-protein (plastocyanins (Pc), azurins, stellacyanin, *etc.*) and intra-protein scale (laccase, ascorbate oxidase, nitrite reductase (NiR), ceruloplasmin, *etc.*).*(1,2)* Oxidized blue copper centers exhibit spectro-physical properties which distinguish them from "normal" (small molecule) Cu(II) complexes:*(3-5)* an intense ($\varepsilon_{max} \approx 3000$-$6000$ M^{-1} cm^{-1}) "blue" absorption band at ~600 nm where normal cupric complexes usually have weak Laporté forbidden d→d transitions with $\varepsilon_{max} \approx 40$ M^{-1} cm^{-1}, EPR spectra showing a ~2-fold reduction in the $A_{\|}$ hyperfine interaction, and higher reduction potentials. Further, these sites facilitate rapid electron transfer over distances of ~13 Å.*(6)* These features reflect an electronic structure in the blue Cu site which is uniquely suited to the protein's function. Reduced cuprous complexes are often tetrahedral while cupric complexes are often tetragonal due to the Jahn-Teller effect. The differences between normal and blue Cu(II) centers have been used to support the existence of a "rack" or "entatic" state in bioinorganic chemistry.*(7-9)* In an entatic/rack state the protein imposes an unusual geometry on the active site which enhances its reactivity.*(7-9)* In blue Cu proteins, the protein rack (or entatic state) can be thought of as opposing the Jahn-Teller distortion, thus effecting little geometric change upon oxidation facilitating rapid electron transfer.

Here we summarize four areas of blue Cu research which are presented in full elsewhere.*(3,10-13)* First, the spectral features resulting from the d^9 oxidized blue Cu ground state wavefunction are well understood.*(3,10)* This half-occupied orbital participates in electron transfer which is facilitated by a high degree of covalency anisotropically distributed along one Cu-ligand bond (the cysteine). Second, we have developed variable energy photoelectron spectroscopy to probe the reduced d^{10} site, which is not accessible to a majority of bioinorganic spectroscopic methods.*(11)* These experiments, in conjunction with SCF-Xα-SW calculations, define the electronic structure of the reduced blue Cu center in relation to normal Cu complexes.*(11)* This study indicates that the protein imposes a long thioether bond on the Cu center. Third, we have evaluated the changes in electronic structure which occur on oxidation of the reduced site to determine the associated change in the geometric structure which would occur at an unconstrained blue Cu center.*(11)* These results are analyzed in the context of rack/entatic state models. Finally, we have studied a perturbed blue Cu protein (NiR) which exhibits dramatically altered spectral features that reflect a perturbed ground state wavefunction.*(12)* The electronic structure of oxidized NiR is compared to that of Pc to explore further the influence of the rack/entatic state in the perturbed relative to classic blue Cu sites.

THE OXIDIZED BLUE CU SITE: ELECTRONIC STRUCTURE AND ELECTRON TRANSFER PATHWAYS

* Author to whom correspondence should be addressed.

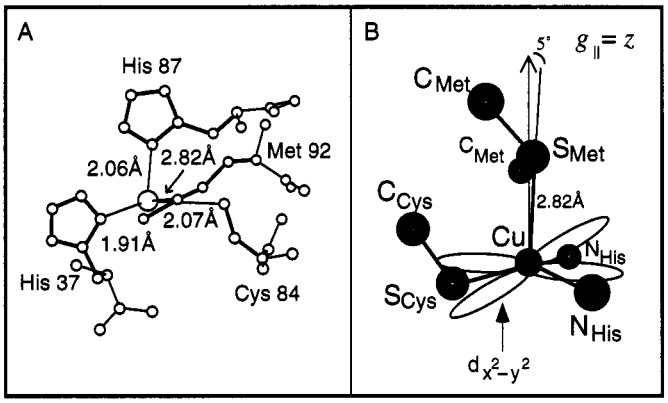

Fig. 1. (A) X-ray structure of the blue Cu in plastocyanin (adapted from Ref. 14). (B) Orientation of $g_{\|}$ and the $d_{x^2-y^2}$ orbital in plastocyanin superimposed on the blue Cu site.

In 1978 Hans Freeman *et al.* presented the first crystal structure of the blue copper site in oxidized Pc.*(15)* Advanced crystallographic techniques have enabled these researchers to achieve a resolution of 1.33 Å, making it one of the best protein crystal structures presently available.*(14)* This structure is shown in Fig. 1A.*(14)* Rather than the normal tetragonal geometry of Cu(II), the Pc active site has a distorted tetrahedral structure with two especially interesting bonds. A short thiolate S–Cu(II) bond at 2.07 Å with cysteine (Cys) 84 and a long thioether S–Cu(II) bond at 2.82 Å to methionine (Met) 92. The other two ligands are fairly normal imidazole N–Cu(II) bonds of histidine (His) residues. Fig. 2 presents the unique spectral features of the blue copper site associated with this unusual geometric structure.*(3-5)* The absorption (Abs) spectrum in Fig. 2A exhibits an extremely intense band at 600 nm. In the electron paramagnetic resonance (EPR) spectrum shown in Fig. 2B, the parallel hyperfine ($A_{\|}$) splitting of the blue copper site is significantly reduced. As will be shown below, these unique spectral features reflect a novel ground state wavefunction. This half-occupied redox active Cu(II) HOMO plays a key role in the electron transfer function of this site.*(3,4,16)*

As can be seen in from the EPR in Fig. 2B, $g_{\|} > g_{\perp} > 2.00$ for the blue copper site which from ligand field theory indicates that the half occupied orbital is $d_{x^2-y^2}$. The orientation of this orbital in the distorted protein site was determined to be perpendicular to the Cu-S_{Met} bond with single crystal EPR spectroscopy.*(17)* Fig. 1B shows that the $g_{\|}$ direction is ~5° from the long thioether S–Cu(II) bond and consequently, the redox active $d_{x^2-y^2}$ orbital is within 15° of the plane defined by the three equatorial strong ligands; the thiolate S and two imidazole N's.

In addition to the small $A_{\|}$ value observed in Pc, small $A_{\|}$ values are observed in a number of distorted tetrahedral copper complexes, in particular D_{2d}-$CuCl_4^{2-}$. An explanation where the distorted D_{2d} geometry allows Cu $4p_z$ to mix into the $d_{x^2-y^2}$ orbital was developed to explain this reduction in $A_{\|}$.*(18)* However, a combination of ligand field calculations*(17)* and low temperature MCD data*(19)* (*vide infra*) provided a d orbital splitting pattern that is associated with an elongated, C_{3v} distorted tetrahedral structure. Such a distortion involves an elongation of one ligand-metal bond with the metal dropped toward the opposing trigonal face. This geometry for the blue Cu site, where the C_3 axis would correspond to the long thioether

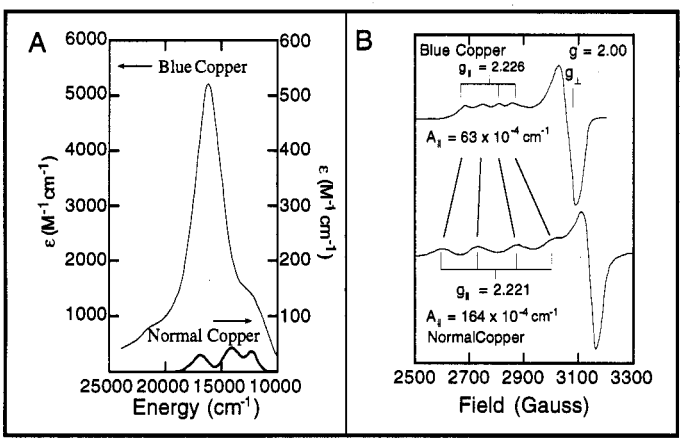

Fig. 2. (A) Abs spectrum of plastocyanin (left ε scale) and "normal" D_{4h}-$CuCl_4^{2-}$ (right ε scale). (B) X-band EPR spectrum of plastocyanin and D_{4h}-$CuCl_4^{2-}$.

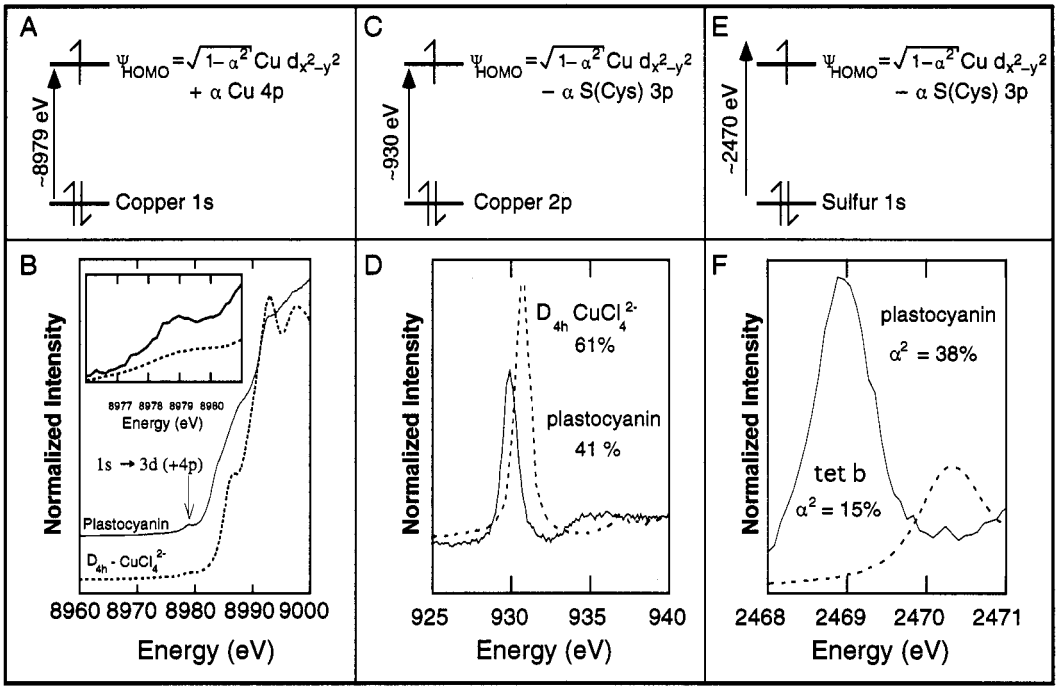

Fig. 3. X-ray Absorption Spectroscopy (XAS) of plastocyanin at multiple energies: (A,C,E) Energy level diagrams depicting the Cu 1s, Cu 2p, and S 1s → HOMO transitions, respectively. (B) polarized single crystal Cu K-edge XAS spectra for poplar plastocyanin (spectra taken from Ref. 20). (D) Orientation averaged Cu L_3-edge XAS spectra for D_{4h}-$CuCl_4^{2-}$ and plastocyanin (spectra taken from Ref. 21). Values listed are the amount of Cu d character in the HOMO. (F) Orientation averaged S K-edge XAS spectra for tet *b* and plastocyanin (spectra taken from Ref. 22). Values are the amount of S 3p character in the HOMO.

S–Cu bond, conflicts with the explanation for small $A_{\|}$ above because in C_{3v} symmetry the Cu $4p_{x,y}$ orbitals, rather than $4p_z$, are of appropriate symmetry to mix with the $d_{x^2-y^2}$ orbital.

To experimentally address this issue we increased the photon energy by ~10 orders of magnitude, analyzing polarized single-crystal Cu K-edge XAS data to determine the nature of this mixing in the Pc HOMO (*i.e.*, $4p_z$ or $4p_{x,y}$).*(23)* The dipole allowed s→HOMO transition will give intensity to a pre-edge feature at 8979 eV corresponding to the amount of p character in the HOMO. The single-crystal XAS spectrum of Pc taken with the E vector oriented along this *z* axis (Fig. 1B) shows no such pre-edge intensity as seen in Fig. 3B. This is the orientation for observing $4p_z$ mixing into the $d_{x^2-y^2}$ orbital and thus there is no measurable $4p_z$ character in the HOMO of Pc. Alternatively, the polarized XAS spectrum taken with the E vector of light in the *xy* plane which would show the $4p_{x,y}$ mixing (plus a quadrupole component) shows considerable the 8979 eV peak intensity. This indicates that the Cu $d_{x^2-y^2}$ orbital only mixes with Cu $4p_{x,y}$ in the blue copper site and thus the origin of the small $A_{\|}$ value is not Cu $4p_z$ mixing. This extremely important result allowed us to focus on an alternative mechanism for small hyperfine splitting: a highly covalent site.*(19,24)* Covalency reduces $A_{\|}$ by delocalizing the electron spin off the metal center and reducing its interaction with the nuclear spin on the copper. Due to the importance of this redox active orbital in biological function we have evaluated the possibility of a highly covalent ground state using spectral methods covering many energy regions.

An electric dipole allowed Cu 2p→half occupied HOMO excitation (the Cu-L edge) gives a transition at ~930 eV (Fig. 3C), whose intensity reflects the amount of Cu $3d_{x^2-y^2}$ character in the HOMO.*(21)* As determined from the data in Fig. 3D, the blue copper site has 0.67 of the Cu L-edge intensity of square planar $CuCl_4^{2-}$. Studies on the latter complex have indicated that it has 61% Cu $d_{x^2-y^2}$ character in the ground state. Thus the intensity ratio of the L_3 edges in Fig. 3D gives ~41% Cu $d_{x^2-y^2}$ character in Pc. Such a reduction in Cu character to the HOMO accounts for the small $A_{\|}$ value observed with EPR. Sulfur K-edge spectral studies demonstrated that this blue Cu covalency dominantly involves the thiolate S–Cu(II) bond.*(25)* The S 1s→half occupied HOMO transition occurs at ~2470 eV (Fig. 3E). The allowed electric dipole component is S 1s→S 3p and thus the intensity of this transition reflects S 3p character in the half occupied HOMO. As can be seen from Fig. 3F, Pc has 2.6 times the intensity of the pre-edge feature in tet *b*,*(26)* a model complex that has a fairly normal thiolate S–Cu(II) bond with ~15% covalency. Thus the intensity ratio from Fig. 3F indicates that the blue copper ground state wavefunction has ~38% thiolate S character.

The final key feature of the ground state wavefunction, its orientation in the *xy* plane, was determined from the assignment of the unique Abs spectrum of the blue copper site. By examining a combination of low

temperature (LT) Abs, circular dichroism (CD) and magnetic circular dichroism MCD which are each governed by a different selection rule,*(12,19)* a minimum of eight transitions are required to fit the absorption spectrum, labeled bands 1 - 8 in Fig. 4A. Band 4 is the intense 600 nm absorption feature characteristic of blue copper sites, and at lower energy, band 6 also has moderate intensity. Polarized absorption data on single crystals of Pc*(17)* show that both bands have the same polarization ratio which associates these with the cysteine-copper bond. As depicted in Fig. 4B, normal Cu(II) complexes exhibit a characteristic charge transfer pattern consisting of a low energy weak π and a high energy intense σ charge transfer transition. This derives from the fact that charge transfer intensity reflects the overlap of the orbitals involved in the transition. In normal Cu(II) complexes (Fig. 4B, top), a lobe of the $d_{x^2-y^2}$ orbital is oriented along the ligand-metal bond and thus the ligand σ orbital, which is at high energy due to the σ bonding, also has the most charge transfer intensity due to overlap. Thus the blue copper absorption spectrum has historically been assigned as band 6 being the cysteine π and band 4 the cysteine $\sigma \rightarrow$Cu(II) $d_{x^2-y^2}$ charge transfer transitions.*(27)* Significant insight into this possible assignment came from LT MCD data*(19)* shown at the bottom of Fig. 4A. Bands 5 to 8 which are all relatively weak in absorption are the most intense in the LT MCD spectrum. LT MCD involves a *C*-term mechanism which requires spin-orbit coupling hence d orbital character. Thus bands 5 to 8 are d$\rightarrow$d transitions with the specific assignments indicated at the top of the low temperature absorption spectrum. Band 4 which is intense in the absorption spectrum is relatively weak in the LT MCD spectrum and thus is assigned as the lowest energy cysteine $\pi \rightarrow$Cu $d_{x^2-y^2}$ charge transfer transition. A higher energy, weak band is associated with the cysteine $\sigma \rightarrow$Cu $d_{x^2-y^2}$ charge transfer transition. (Note that the Cys σ here refers to the pseudo σ valence orbital (see Fig. 6B *vide infra*) and the moderate absorption intensity in band 6 derives from the fact that it involves the d_{xz+yz} orbital which has some mixing with the cysteine π orbital).*(19)* Thus, Pc does not exhibit the normal low energy weak and high energy intense charge transfer pattern of most cupric complexes (Fig. 4B, top), and since charge transfer intensity derives from overlap the blue copper intensity pattern (π intense/σ weak) requires that the $d_{x^2-y^2}$ orbital be rotated by 45° such that its lobes are bisected by the S_{Cys}–Cu(II) bond (Fig. 4B, bottom). This rotation of the $d_{x^2-y^2}$ orbital derives from the strong π antibonding interaction with the thiolate sulfur at the unusually short 2.07 Å S_{Cys}–Cu(II) bond length in the blue copper site.

Complementary to these experimental methods, SCF-Xα-SW calculations*(29)* have played an important role in developing our understanding of bonding in the Pc HOMO.*(3)* Very good agreement is obtained between the SCF-Xα-SW calculations and spectral data covering many orders of magnitude in photon energy (*vide supra*)*(3,13)* The calculated ground state wavefunction pictured in Fig. 5 is given in the plane

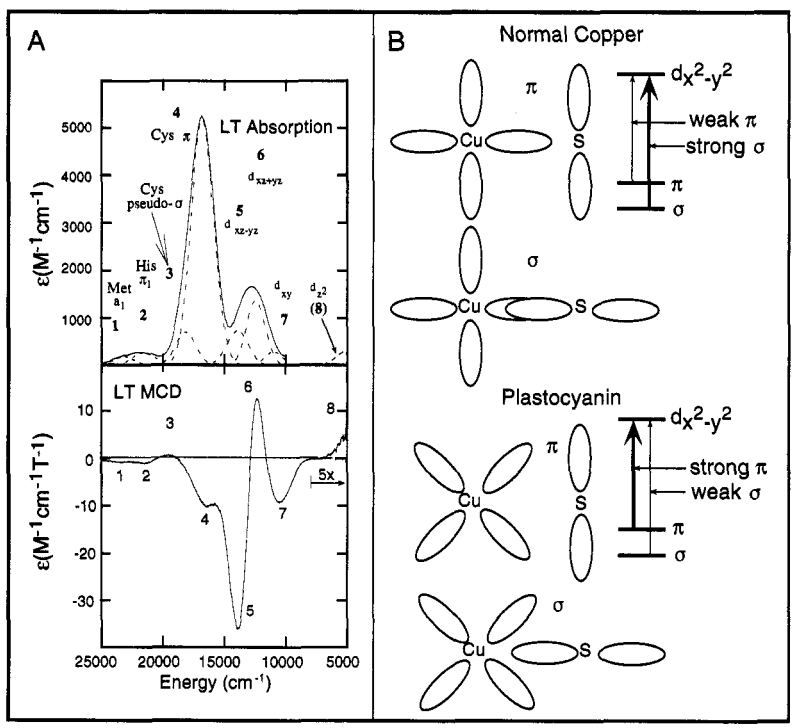

Fig. 4. Blue copper excited-state spectra and orientation of plastocyanin ground state wavefunction. (A) Low-temperature absorption and MCD spectra of plastocyanin. Band 8 has been scaled by a factor of five in the MCD spectrum. The LT absorption spectrum has been Gaussian resolved into its component bands as in Ref. 19. (B) Cu–cysteine bonding interactions; top section illustrates a "normal" bonding mode with weak π and strong σ charge transfer transitions while the bottom section depicts the strong π and weak σ charger transfer spectra in plastocyanin (which results from a 45° rotation of the Cu $d_{x^2-y^2}$ orbital due to strong π bonding). Note that the σ here refers to to the pseudo σ valence orbital (see Fig. 6B).

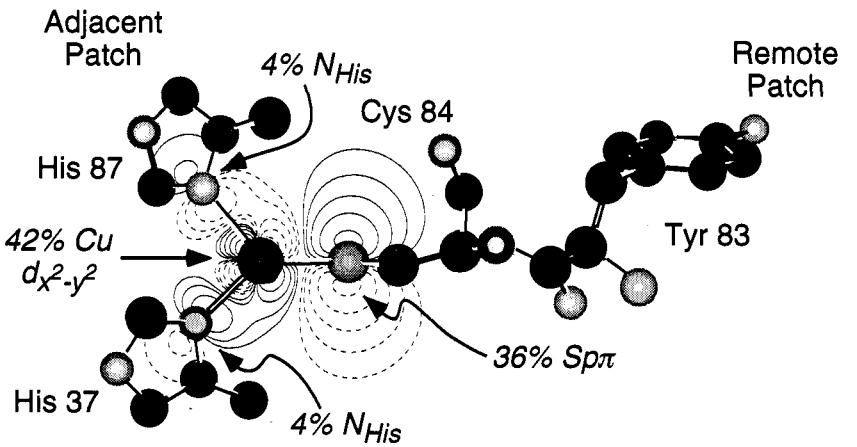

Fig. 5. Redox active orbital in Pc as calculated by SCF-Xα-SW calculations superimposed on a proposed long-range electron transfer pathway in blue copper proteins.*(3,4,28)* Shown here is the specific path in plastocyanin that is activated by the covalency of the $S_{p\pi}$ orbital for electron transfer to the remote patch at ~12.5 Å from the blue copper site. The low-energy, intense Cys $S_{p\pi} \rightarrow$ Cu charge transfer transition provides an effective hole superexchange mechanism for rapid long-range electron transfer between these sites. The structure has been taken from Ref. 14 and is drawn with the *xy* plane in the paper.

perpendicular to the Cu–S_{Met} bond containing the Cu-S_{Cys} bond and the two N_{His} ligands. It is extremely interesting in that it is highly covalent with only 42% Cu $d_{x^2-y^2}$ character and strongly anisotropic with 36% character from the $S_{p\pi}$ orbital of the cysteinate sulfur.*(12,19,24)* The calculated covalencies are in good agreement with Cu and S covalencies measured experimentally above. The calculations also indicate that the Cu-S_{Cys} bond is of the novel π-type as suggested by the analysis of the Abs, CD, and MCD spectroscopic results and reproduce the ground state *g* values reasonably well.

We have correlated this ground-state wavefunction with the crystal structures of several blue copper proteins to obtain significant insight into its contribution to long range ET pathways.*(3,16)* In Pc, the ligated Cys is adjacent to a surface exposed Tyr in the remote patch of the protein through which intraprotein ET can occur. In multicopper proteins such as laccase and nitrite reductase,*(33,34)* the covalent Cys is flanked by His residues which ligate another Cu that is used in enzymatic function of the active site. In Fig. 5 a portion of the Pc crystal structure*(14)* has been overlaid on the calculated wavefunction and shows the highly anisotropic covalency of the Cu-S_{Cys} bond that activates this ligand for highly directional long-range ET by a Cys-His (or a Cys-Tyr) pathway, while the intense, low-energy Cys π → Cu charge transfer transition provides an efficient hole superexchange mechanism for rapid ET through this pathway.*(16)* Thus, while the unique spectral features of the blue copper center certainly reflect the unusual geometric structure and ligation of the site in Fig. 1A, they, in fact, derive from an electronic structure tuned for rapid electron transfer to a specific position in or on the protein.*(3)*

THE REDUCED BLUE COPPER SITE: LIGAND-METAL BONDING CONTRIBUTION TO REDUCTION POTENTIALS

While determining the unusual spectroscopic features of the oxidized blue Cu site was challenging, the d^{10} configuration of the reduced blue Cu center is inaccessible to the usual array of bioinorganic chemistry spectroscopic techniques and consequently its electronic structure remains less well characterized. To better define this site, we have been developing variable energy photoelectron spectroscopy (PES) using synchrotron radiation to define the bonding and its change with ionization (*i.e.*, oxidation) in transition metal complexes.*(35-37)* Since we are interested in electrons emitted from valence orbitals involved in bonding, we study model complexes rather than the proteins, and since we want to understand normal ligand-metal bonding and its relation to the blue copper site, the models we have chosen to study are the blue copper relevant imidazole, dimethylsulfide and methylthiolate ligands bound to coordinatively unsaturated Cu(I) sites on oxide and chloride single crystal surfaces in ultra-high vacuum. As an example, the photoelectron spectral data for methylthiolate bound to cuprous oxide is shown in Fig. 6A (where we have used the surface oxide to deprotonate methylthiol).*(38)* The dashed spectrum gives the valance band region of clean Cu_2O, and the solid spectrum is that of methylthiolate bound to the surface. The difference spectrum at the bottom gives the valance orbitals of the thiolate–Cu(I) bond. Varying the photon energy changes the intensity of the peaks*(39,40)* and allows the specific assignments of the levels indicated in the difference spectrum. The three valence thiolate orbitals involved in bonding to the Cu(I) are the π, pseudo σ and σ shown in Fig. 6B. The π and pseudo σ, which are the sulfur p orbitals perpendicular to the S–C bond, dominate the bonding and split in energy as the Cu-S-CH_3 angle φ in Fig. 6B deviates from 180°. Thus the energy splittings and intensity changes with photon energy of the peaks in the difference spectrum in Fig. 6A give the geometric and electronic structure of the unconstrained thiolate–Cu(I) bond of the surface complex. Our strategy was to use variable energy PES to experimentally define the geometric and

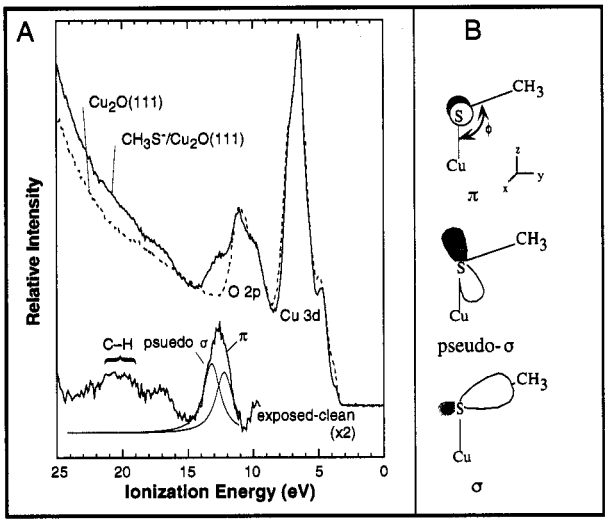

Fig. 6. CH_3S–Cu(I) bonding. (A) Valence band PES of clean $Cu_2O(111)$, $Cu_2O(111)$ exposed to methanethiol, and their difference spectrum with Gaussian/Lorenzian resolution of the low-energy region. (B) Valence orbitals of methanethiolate. Spectra from Ref. 11.

electronic structure of each normal ligand–Cu(I) bond for the surface complexes. We then use these data to evaluate and calibrate SCF-Xα–SW electronic structure calculations of the unconstrained surface complexes. These experimentally calibrated calculations were then used to generate an electronic structure description of the reduced blue copper site and to evaluate the change in electronic structure with oxidation.

These studies, which are described in detail in Ref. 11, demonstrate that the bonding in the reduced blue copper site is dominated by ligand p to Cu(I) 4p donor interactions. Thus, even though the bonding involves a reduced copper center which results in the d orbitals being higher in energy by 1 to 2 eV due to the lower effective nuclear charge on the copper relative to the oxidized site, there is no evidence for back-bonding for any of the blue copper ligands. We further have found that the long thioether S_{Met}–Cu(I) bond length of 2.8 Å does not derive from the electronic structure of the reduced blue copper site, but is imposed on the site by the tertiary structure of the protein. As will be described in the next section, this appears to be the only feature of the blue copper site structure that can be ascribed to an entatic or rack state. This elongated thioether S_{Met}–Cu(I) bond reduces the donor interaction of this ligand with the copper. This is compensated for by the thiolate leading to the short strong S_{Cys}–Cu(I) bond (Fig. 7A). The long thioether S_{Met}–Cu bond destabilizes the oxidized site more than the reduced site and is found to be the dominant ligand contribution to the high reduction potential of the blue copper center. This is referenced to the potential of a tetraimidazole complex, bis[2,2'-bis(2-imidazolyl)biphenyl] copper,*(41)* where the imidazoles are constrained by bridging groups to undergo only a limited geometric change on oxidation as is observed for the blue copper site (*vide infra*). This geometric constraint also contributes the to high reduction potential of the copper site.

Change in Electronic Structure on Oxidation: Contributions to Geometry

Comparison of the electronic structure descriptions of the oxidized and reduced blue copper sites indicates that the ligand donor interactions with the unoccupied copper 4p (and 4s) levels change little upon oxidation

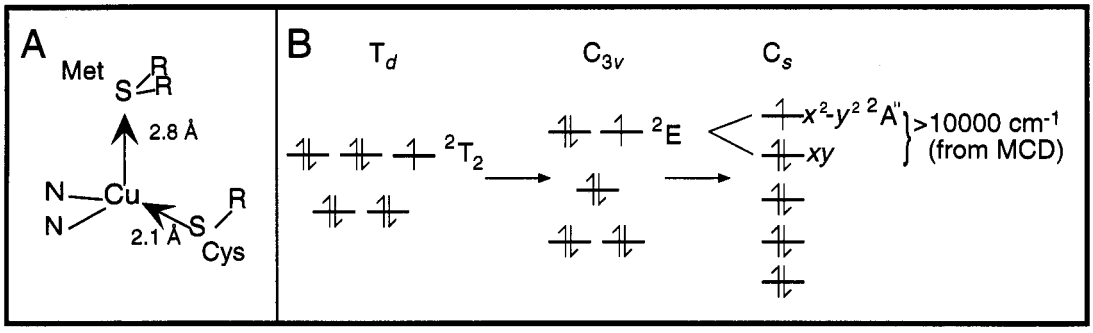

Fig. 7. (A) Axial ligand effects in plastocyanin. The long S_{Met}–Cu(I) bond is imposed by the tertiary protein structure on the blue copper site and results in a shortening of the S_{Cys}–Cu(I) bond. (B) Possilbe Jahn-Teller distorting forces in the blue Cu sites. The large splitting of the $d_{x^2-y^2}$ and d_{xy} by the site structure eliminates the Jahn-Teller effect.

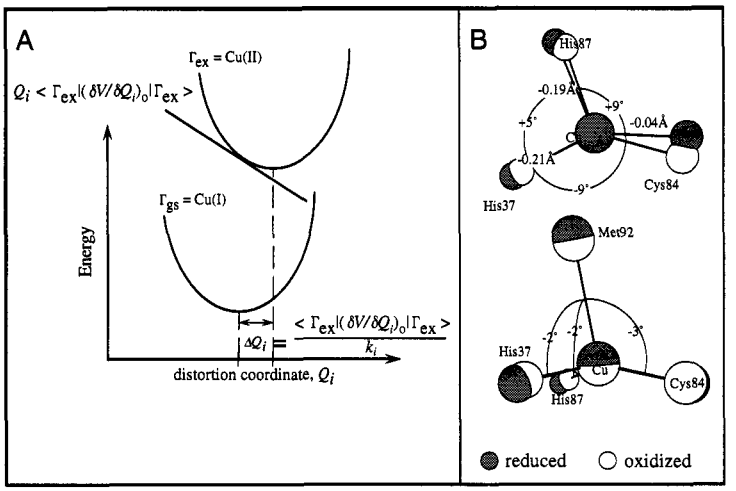

Fig. 8. Distorting forces and geometric changes in the blue copper site on oxidation. (A) Configuration coordinate diagram of the linear coupling term for the distorting force along the *i*th normal mode of vibration, Q_i, on the oxidized Cu(II) site relative to the reduced Cu(I) ground state. δV is the energy change calculated for a distortion δQ_i of the molecule. ΔQ_i is the expected distortion along the normal mode for the calculated linear coupling term. (B) Crystallographically determined structural changes in the bond lengths and angles in the equatorial plane (left) and in the $S_{Met}CuL$ angles (right) (taken from Refs. 42 and 14).

and that the dominant change in bonding involves the hole produced in the $d_{x^2-y^2}$ derived HOMO in Fig. 5. Thus, on oxidation, the blue copper site loses a strong antibonding interaction with the thiolate sulfur and weaker antibonding interactions with the imidazole nitrogens.*(11)*

Having obtained an experimentally calibrated electronic structure description of the reduced site, we could evaluate the changes in geometric structure which would occur for a blue copper site unconstrained by the protein. This involves evaluation of the electron-nuclear linear coupling terms of the oxidized site in the reduced geometry along all the normal modes, Q_i, of the blue copper site. As illustrated in Fig. 8A, a non-zero slope of the linear coupling term of the oxidized site in the reduced geometry, $Q_i <\Gamma_{ex}|(\delta V/\delta Q_i)_o|\Gamma_{ex}>$, corresponds to a distorting force along normal mode Q_i.*(39,43)* The significant distorting forces we find to be present are consistent with the change in electronic structure on oxidation described above. There is a large distorting force toward contraction of the thiolate S_{Cys}–Cu bond. This, however, is opposed by a large force constant, k_i, associated with the short, strong S_{Cys}–Cu bond leading to only limited contraction ($\Delta Q_i = <\Gamma_{ex}|(\delta V/\delta Q_i)_o|\Gamma_{ex}>/k_i$). There are also distorting forces along the N(His)–Cu bonds. Fig. 8B depicts the geometric structural changes on oxidation of a blue copper site determined through crystallography.*(14,44)* Consistent with the linear coupling terms, the thiolate S_{Cys}–Cu bond contracts by 0.04 Å on oxidation. The N_{His}–Cu bonds are found from crystallography to contract by 0.2 Å,*(14,44)* while from extended X-ray absorption fine structure (EXAFS) this contraction is more limited at 0.07 Å.*(23,45)* Importantly, no significant distorting force is present in any of the bending modes and no significant angle change is observed in the crystal structures with oxidation of the blue copper site in Pc.

An entatic or rack state where the Cu(I) geometry is imposed on the Cu(II) site by the protein would correspond to a large Jahn-Teller distorting force along a bending mode. The lack of a Jahn-Teller distorting force in the oxidized blue copper site can be understood from the scheme in figure 7B. In an idealized tetrahedral structure there would be a $^2T_2$ ground state which is orbitally degenerate and this leads to the Jahn-Teller distortion. In the reduced blue copper site there is an elongated thioether S–Cu bond which produces C_{3v} effective symmetry at the copper leading to a ^2E ground state in the oxidized site which corresponds to the unpaired electron being in the degenerate ($d_{x^2-y^2}$, d_{xy}) set of orbitals. The long thioether S–Cu bond further results in contraction of the thiolate S–Cu bond (*vide supra*) which splits the orbital degeneracy of the ^2E. In particular, from the MCD assignment in Fig. 4A the d_{xy} level is > 10,000 cm^{-1} above the $d_{x^2-y^2}$ ground state; it is a linear coupling term between these levels that would lead to a Jahn-Teller distorting force. Thus there is little geometric change on oxidation and a low Franck-Condon barrier to electron transfer.*(6,14)*

THE PERTURBED BLUE CU SITE IN NITRITE REDUCTASE: PERTURBED ELECTRONIC STRUCTURE AND THE ENTATIC STATE :

Based on spectral properties, the diverse group of proteins containing blue copper sites can be differentiated into a dominant class which includes Pc and has an intense peak at ~600 nm and axial EPR spectra, and a perturbed class which exhibits increased absorption at ~450 nm and a rhombic EPR signal.*(12)* Nitrite reductase from *Achromobacter cycloclastes* (NiR) appears to represent a limit on the continuum of spectral perturbations exhibited by the second class. Fig. 9A comprares the Abs spectrum of NiR, which is characterized by the intense band at ~450 nm and weaker band at ~600 nm, to that of the classic blue copper

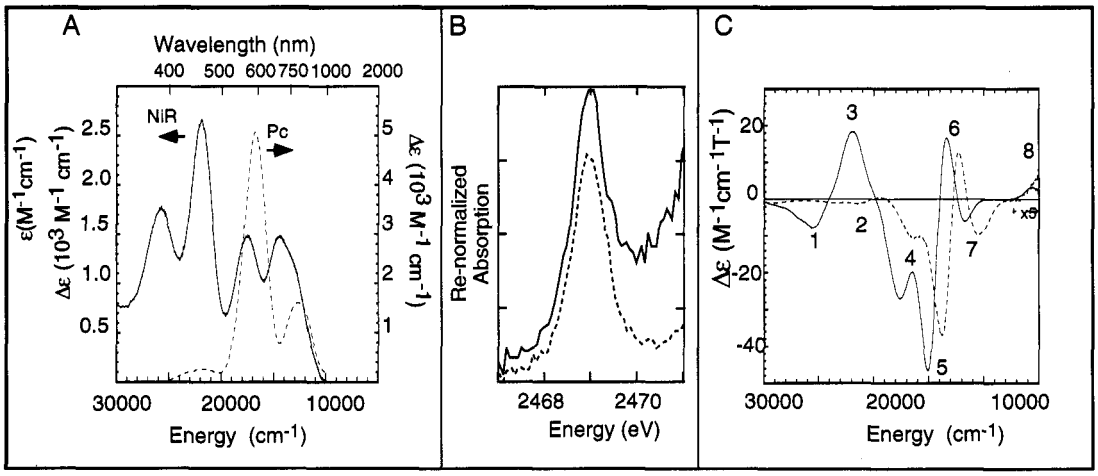

Fig. 9. Comparison of the spectral properties of nitrite reductase (NiR) and plastocyanin (Pc). (A) LT Abs spectra. (B) S K-Edge spectra renormalized to the number of S atoms in each protein (note that the baselines are different). (C) LT MCD spectra. In each panel solid lines are NiR and dashed lines are Pc. Spectra from Ref. 12.

Abs spectrum exhibited by Pc. This intensity redistribution indicates a perturbed electronic structure in NiR compared to that of Pc, which reflects an altered geometry around the blue Cu site in NiR. High resolution crystal structures (< 2 Å) exist for both oxidized proteins*(14,33)* and reveal that in NiR the Cu-S_{Met} distance is much shorter (~2.6 Å) than in Pc. The increased charge donation of the S_{Met} axial ligand in NiR reduces the donor interaction with the S_{Cys} relative to Pc. Accordingly, a weaker Cu-S_{Cys} bond is observed in the crystal structure*(33)* and implied by the decrease from 420 cm^{-1} (in Pc)*(46,47)* to 360 cm^{-1} (in NiR)*(48)* in the Cu-S_{Cys} vibrational frequency observed with resonance Raman.*(49)* Based on these observations the Cu-S_{Cys} bond in NiR is expected to be less covalent than that in Pc.

Fig. 9B compares the pre-edge regions of the S K-edge XAS spectra of Pc and NiR which provides directly measured values of 38 ± 1.2% (Pc) and 39 ± 1.4% (NiR) for the total S 3p covalency in the HOMO.*(12)* Since the Cu-S_{Cys} bond in NiR is weaker and less covalent than the analogous bond in Pc the equivalent S character in the HOMOs indicates the presence of an additional contribution to the S-Cu covalency in NiR. This must reflect the fact that S_{Met} character has mixed into the HOMO in addition to S_{Cys} character.

Since in Pc the $d_{x^2-y^2}$ HOMO is nearly perpendicular to the Cu-S_{Met} direction, the HOMO must be rotated in NiR to exhibit such S_{Met} character. Such a rotation would be consistent with a significant tetragonal distortion of the approximately tetrahedral structure of the classic blue Cu site. The ~1000 cm^{-1} shift to higher energy for each Cu(II) d-d transition in NiR, observed with LT MCT in Fig. 9C, provides evidence of such a tetragonal distortion. If the electronic structure distortion in NiR were tetrahedral, the d-d transition energies would decrease.

This HOMO rotation is also consistent with the dramatic intensity redistribution in the charge transfer (CT) Abs spectra in Fig. 9A. In NiR the intensity of the Cys $S_{p\sigma}$-Cu LMCT band at ~450 nm increases (to become most intense) at the expense of the Cys $S_{p\pi}$-Cu LMCT band at ~600 nm (which is most intense in Pc). Thus the Cu-S_{Cys} interaction in NiR differs from that in Pc by mixing in significant σ-type overlap (Fig. 4B top). The integrated intensity of the both S_{Cys}-Cu LMCT bands is less in NiR that Pc, supporting the presence of a less covalent Cu-S_{Cys} bond. The rotated Cu orbital in NiR has increased overlap with S_{Met}, which is manifested by significantly increased intensity in the Cu-S_{Met} LMCT band at ~25600 cm^{-1} as seen in Fig. 9A.

Xα-SW calculations support a tetragonally rotated orbital in the HOMO of NiR and have allowed us to explore further this rotation.*(12)* Fig. 10 shows contours of the HOMO through two different planes. A comparison of Fig. 5 with 10A shows the rotation of the HOMO and the increased $S_{p\sigma}$ character in the Cu-S_{Cys} interaction while Fig. 10B shows significant electron density along the Cu-S_{Met} direction, a direction which shows little electron density in Pc. The HOMO of NiR shows 48% Cu d character, similar to that in Pc, as is the 7% N_{His} covalency. The calculations indicate that this orbital rotation does effect a redistribution of covalency between S_{Cys} and S_{Met} as the S_{Cys} 3p character in the HOMO is significantly reduced from 35% in Pc to 28% in NiR while the S_{Met} 3p character increases from ~0% in Pc to 6% in NiR. This calculated covalency description for NiR is consistent with both the S K-edge XAS pre-edge features, the LT MCD features, and the decreased Cu-S_{Cys} covalency expected from resonance Raman*(48)* and crystallography.*(33)*

Tetrahedral Cu(II) complexes typically undergo a Jahn-Teller tetragonal distortion.*(50)* However, for Pc, as described above, the long, protein-imposed Cu-S_{Met} bond and concomitantly short Cu-S_{Cys} bond lower the site symmetry to approximately C_s, breaking the d_{xy} and $d_{x^2-y^2}$ orbital degeneracy, which would

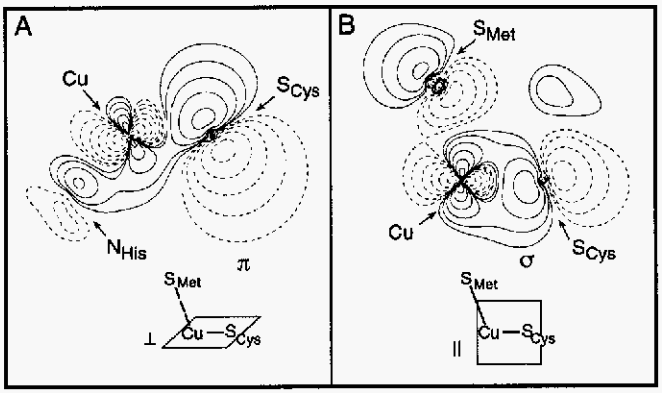

Fig. 10. Contours of the half-filled, redox active HOMO in NiR plotted perpendicular (A) and parallel (B) to the S_{Met}–Cu–S_{Cys} plane.

otherwise lead to the Jahn-Teller distorting force.*(12)* Distorting the Pc site structure by decreasing the Cu-S_{Met} and increasing Cu-S_{Cys} distances as observed in NiR would initially result in a tetrahedral distortion which decreases the splitting between the Cu d_{xy} and $d_{x^2-y^2}$ orbitals. This would make such a Cu(II) site susceptible to a further tetragonal distortion along a Jahn-Teller active normal coordinate, in particular the ε(u) mode depicted in Fig. 11A. Thus, at the blue Cu site in NiR, the short Cu-S_{Met} bond will induce a further Jahn-Teller tetragonal distortion which can be characterized by twisting the plane containing S_{Met}-Cu-S_{Cys} with respect to the plane containing N_{His}-Cu-N_{His} (11B,C). It is this tetragonal distortion, **not** a tetrahedral distortion,*(49,51)* which perturbs the electronic structure of NiR relative to Pc by mixing significant σ character into the Cu-S_{Cys} interaction and adding S_{Met} character into the HOMO which decrease the covalency of the Cu-S_{Cys} interaction. Using the ideas of the protein rack/entatic state developed in the last section, the tetragonal distortion in NiR implies that the protein matrix surrounding the blue Cu center is less entatic than that in Pc.*(12)* The reduced entatic nature of the blue Cu center in NiR and the associated decrease in S_{Cys} covalency, should have significant implications for electron transfer reactivites of perturbed blue Cu centers.

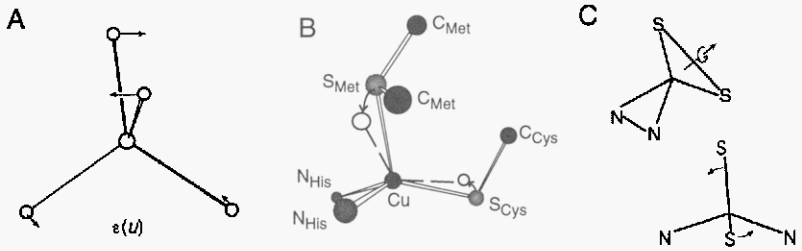

Fig 11. (A) The Jahn-Teller active ε(u) mode for tetrahedral geometries. (B) Superposition of the NiR (white spheres and dashed bonds) and Pc (solid spheres and bonds) active sites emphasizing the ε(u)-type tetragonal distortion to give a more square planar geometry in NiR. (C) Stick figures representing the relative motions of the N_{His}–Cu–N_{His} and S_{Met}–Cu–S_{Cys} planes.

CONCLUDING COMMENTS

The unique spectral features of the oxidized blue copper site derive from the high anisotropic covalency of the ground state wavefunction involving the thiolate which activates this ligand as an efficient superexchange pathway for long range electron transfer. Variable energy photoelectron spectroscopy combined with SCF-Xα-SW calculations have been used to determine the electronic structure of the reduced blue copper site for the first time and to evaluate the change in electronic structure which occurs upon oxidation. This change in electronic structure is consistent with the limited geometric structural change observed leading to a low Franck-Condon barrier to electron transfer. Thus the reduced geometry is not imposed on the oxidized site by the protein. The entatic or rack state in blue copper proteins would appear to involve the protein tertiary structure imposing the long methionine S–Cu bond on the reduced site. This leads to the high reduction potential, the short thiolate S–Cu bond and therefore the efficient superexchange pathway and the lack of a Jahn-Teller distorting force in the oxidized site which results in little geometric change and rapid electron transfer. Perturbed spectral features are observed when the Cu site undergoes an tetragonal ε(u)-like distortion which results from a less constrained entatic/rack state in the protein.

ACKNOWLEDGMENTS

EIS would like to thank his students and collaborators for their contributions and commitment to this research. This work has been supported by the NSF (CHE-9528250).

REFERENCES

(1) Adman, E. T. In *Advances in Protein Chemistry*; C. B. Anfinsen, F. M. Richards, J. T. Edsall and D. S. Eisenberg, Eds.; Academic Press, Inc: San Diego, 1991; Vol. 42; pp 145.
(2) Adman, E. T. In *Topics in Molecular and Structural Biology: Metalloproteins*; P. Harrison, Ed.; MacMillan: New York, 1985; Vol. 1; pp 1.
(3) Solomon, E. I.; Lowery, M. D. *Science* **1993**, *259*, 1575.
(4) Solomon, E. I.; Baldwin, M. J.; Lowery, M. D. *Chem. Rev.* **1992**, *92*, 521.
(5) Solomon, E. I.; Penfield, K. W.; Wilcox, D. E. *Struct. Bonding (Berlin)* **1983**, *53*, 1.
(6) Sykes, A. G. *Adv. Inorg. Chem.* **1991**, *36*, 377.
(7) Lumry, R.; Eyring, H. *J. Phys. Chem.* **1954**, *58*, 110.
(8) Malmström, B. G. *Eur. J. Biochem.* **1994**, *223*, 711.
(9) Williams, R. J. P. *Eur. J. Biochem.* **1995**, *234*, 363.
(10) Solomon, E. I.; Lowery, M. D. In *The Chemistry of Copper and Zinc Triads*; S. K. Chapman A. J. Welch, Ed.; The Royal Society of Chemistry: Cambridge, 1993; pp 12.
(11) Guckert, J. A.; Lowery, M. D.; Solomon, E. I. *J. Am. Chem. Soc.* **1995**, *117*, 2817.
(12) LaCroix, L. B.; Shadle, S. E.; Wang, Y.; Averill, B. A.; Hedman, B.; Hodgson, K. O.; Solomon, E. I. *J. Am. Chem. Soc.* **1996**, *118*, 7755.
(13) Solomon, E. I.; Penfield, K. W.; Gewirth, A. A.; Lowery, M. D.; Shadle, S. S.; Guckert, J. A.; LaCroix, L. B. *Inorg. Chim. Acta* **1996**, *243*, 67.
(14) Guss, J. M.; Bartunik, H. D.; Freeman, H. C. *Acta Crystallogr.* **1992**, *B48*, 790.
(15) Colman, P. M.; Freeman, H. C.; Guss, J. M.; Murata, M.; Norris, V. A.; Ramshaw, J. A. M.; Venkatappa, M. P. *Nature* **1978**, *272*, 319.
(16) Lowery, M. D.; Guckert, J. A.; Gebhard, M. S.; Solomon, E. I. *J. Am. Chem. Soc.* **1993**, *115*, 3012.
(17) Penfield, K. W.; Gay, R. R.; Himmelwright, R. S.; Eickman, N. C.; Norris, V. A.; Freeman, H. C.; Solomon, E. I. *J. Am. Chem. Soc.* **1981**, *103*, 4382.
(18) Bates, C. A.; Moore, W. S.; Standley, K. J.; Stevens, K. W. H. *Proc. Phys. Soc.* **1962**, *79*, 73.
(19) Gewirth, A. A.; Solomon, E. I. *J. Am. Chem. Soc.* **1988**, *110*, 3811.
(20) Scott, R. A.; Hahn, J. E.; Doniach, S.; Freeman, H. C.; Hodgson, K. O. *J. Am. Chem. Soc.* **1982**, *104*, 5364.
(21) George, S. J.; Lowery, M. D.; Solomon, E. I.; Cramer, S. P. *J. Am. Chem. Soc.* **1993**, *115*, 2968.
(22) Shadle, S. E.; Penner-Hahn, J. E.; Schugar, H. J.; Hedman, B.; Hodgson, K. O.; Solomon, E. I. *J. Am. Chem. Soc.* **1993**, *115*, 767.
(23) Scott, R. A.; Hahn, J. E.; Doniach, S.; Freeman, H. C.; Hodgson, K. O. *J. Am. Chem. Soc.* **1982**, *104*, 5364.
(24) Penfield, K. W.; Gewirth, A. A.; Solomon, E. I. *J. Am. Chem. Soc.* **1985**, *107*, 4519.
(25) Shadle, S. E.; Penner-Hahn, J. E.; Schugar, H.; Hedman, B.; Hodgson, K. O.; Solomon, E. I. *J. Am. Chem. Soc.* **1993**, *115*, 767.
(26) Hughey IV, J. L.; Fawcett, T. G.; Rudich, S. M.; Lalancette, R. A.; Potenza, J. A.; Schugar, H. J. *J. Am. Chem. Soc.* **1979**, *101*, 2617.
(27) Solomon, E. I.; Hare, J. W.; Gray, H. B. *Proc. Natl. Acad. Sci. USA* **1976**, *73*, 1389.
(28) Lowery, M. D.; Guckert, J. A.; Gebhard, M. S.; Solomon, E. I. *J. Am. Chem. Soc.* **1993**, *115*, 3012.
(29) (a) Johnson, K. H. *Adv. Quant. Chem., 7* **1973** 143. (b) Johnson, K. H.; Norman Jr., J. G.; Connolly, J. W. D., in F. Herman, A. D. McLean and R. K. Nesbet (ed.), *Computational Methods for Large Molecules and Localized States in Solids*, Plenum, New York, **1973**, p. 161. (c) Connolly, J. W. D., in G. A. Segal (ed.), *Semiempirical Methods of Electronic Structure Calculations, Part A: Techniques*, Plenum, New York, **1977**. (d) Rosch, N. in P. Phariseu and L. Scheire (ed.), *Electrons in Finite and Infinite Structures*, Wiley, New York, **1977**. (e) Slater, J. C. *The Calculation of Molecular Orbitals*, John Wiley & Sons, New York, **1979**, p. 104.
(30) Solomon, E. I.; Gewirth, A. A.; Cohen, S. L. *Understanding Molecular Properties*; D Reidel: Dordrecht, 1987, pp 27.
(31) Gewirth, A. A.; Cohen, S. L.; Schugar, H. J.; Solomon, E. I. *Inorg. Chem.* **1987**, *26*, 1133.
(32) Didziulis, S. V.; Cohen, S. L.; Gewirth, A. A.; Solomon, E. I. *J. Am. Chem. Soc.* **1988**, *110*, 250.
(33) Adman, E. T.; Godden, J. W.; Turley, S. *J. Biol. Chem.* **1995**, *211*, 27458.
(34) Messerschmidt, A.; Ladenstein, R.; Huber, R.; Bolognesi, M.; Avigliano, L.; Petruzzelli, R.; Rossi, A.; Finazzi-Agro, A. *J. Mol. Biol.* **1992**, *224*, 179.
(35) Lin, J.; Jones, P.; Lowery, M. D.; Gay, R. R.; Cohen, S. L.; Solomon, E. I. *Inorg. Chem.* **1992**, *31*, 686.
(36) Lin, J.; Jones, P.; Guckert, J.; Solomon, E. I. *J. Am. Chem. Soc.* **1991**, *113*, 8312.
(36) Didziulis, S. V.; Cohen, S. L.; Butcher, K. D.; Solomon, E. I. *Inorg. Chem.* **1988**, *27*, 2238.
(38) Lin, J.; May, J. A.; Didziulis, S.; Solomon, E. I. *J. Am. Chem. Soc.* **1992**, *114*, 4718.
(39) Solomon, E. I. *Comm. Inorg. Chem.* **1984**, *3*, 225.
(40) Yeh, J. J. *At. Data Nucl. Data Tables* **1985**, *32*, 1.
(41) Knapp, S.; Keenan, T. P.; Xiaohua, X.; Fikar, R.; Potenza, J. A.; Schugar, H. J. *J. Am. Chem. Soc.* **1990**, *112*, 3452.
(42) Guss, J. M.; Harrowill, P. R.; Murata, M.; Norris, V. A.; Freeman, H. C. *J. Mol. Biol.* **1986**, *192*, 361.
(43) Wilson, R. B.; Solomon, E. I. *J. Am. Chem. Soc.* **1980**, *102*, 4085.
(44) Guss, J. M.; Harrowill, P. R.; Murata, M.; Norris, V. A.; Freeman, H. C. *J. Mol. Biol.* **1986**, *192*, 361.
(45) Murphy, L. M.; Hasnain, S. S.; Strange, R. W.; Harvey, I.; Ingledew, W. J. In *X-ray Absorption Fine Structure*; S. S. Hasnain, Ed.; Ellis Hardwood: Chickester, 1990; pp 152.
(46) Han, J.; Adman, E. T.; Beppu, T.; Codd, R.; Freeman, H. C.; Huq, L.; Loehr, T. M.; Sanders-Loehr, J. *Biochemistry* **1991**, *30*, 10904.
(47) Qiu, D.; Dong, S.; Ybe, J. A.; Hecht, M. H.; Spiro, T. G. *J. Am. Chem. Soc.* **1995**, *117*, 6443.
(48) Han, J.; Loehr, T. M.; Lu, Y.; Valentine, J. S.; Averill, B. A.; Sanders-Loehr, J. *J. Am. Chem. Soc.* **1993**, *115*, 4256.
(49) Andrew, C. R.; Sanders-Lohr, J. *Acc. Chem. Res.* **1996**, *29*, 365.
(50) Jahn, H. A.; Teller, E. *Proc. Roy. Soc. London* **1937**, *A161*, 220.
(51) Andrew, C. R.; Yeom, H.; Valentine, J. S.; Karlsson, B. G.; Bonander, N.; van Pouderoyen, G.; Canters, G. W.; Loehr, T. M.; Sanders-Loehr, J. *J. Am. Chem. Soc.* **1994**, *116*, 11489.